Physics Letters B 820 (2021) 136601

Contents lists available at ScienceDirect

Physics Letters B

www.elsevier.com/locate/physletb

Sensitive search for near-symmetric and super-asymmetric fusion-fission of the superheavy element Flerovium (Z=114)

K. Banerjee [a,*,1], D.J. Hinde [a], M. Dasgupta [a], J. Sadhukhan [b,c], E.C. Simpson [a], D.Y. Jeung [a], C. Simenel [a,d], B.M.A. Swinton-Bland [a], E. Williams [a], L.T. Bezzina [a], I.P. Carter [a], K.J. Cook [a,e], H.M. Albers [f], Ch.E. Düllmann [f,g,h], J. Khuyagbaatar [f,g], B. Kindler [i], B. Lommel [i], C. Mokry [g], E. Prasad [a,2], J. Runke [f,h], N. Schunck [j], C. Sengupta [a], J.F. Smith [a,3], P. Thörle-Pospiech [g,h], N. Trautmann [h], K. Vo-Phuoc [a], J. Walshe [a], A. Yakushev [f,g]

[a] Department of Nuclear Physics, Research School of Physics, The Australian National University, Canberra, ACT 2601, Australia
[b] Variable Energy Cyclotron Centre, 1/AF, Bidhan Nagar, Kolkata-700064, India
[c] Homi Bhabha National Institute, Anushakti Nagar, Mumbai 400094, India
[d] Department of Theoretical Physics, Research School of Physics, Australian National University, Canberra, ACT 2601, Australia
[e] Facility for Rare Isotope Beams, Michigan State University, 640 South Shaw Lane, East Lansing, MI 48824, USA
[f] SHE Chemistry Department, GSI Helmholtzzentrum für Schwerionenforschung, 64291 Darmstadt, Germany
[g] SHE Chemistry Section, Helmholtz Institute Mainz, 55099, Mainz, Germany
[h] Department of Chemistry - TRIGA Site, Johannes Gutenberg-Universität Mainz, 55099, Mainz, Germany
[i] Target Laboratory, GSI Helmholtzzentrum für Schwerionenforschung, 64291 Darmstadt, Germany
[j] Nuclear and Chemical Science Division, Lawrence Livermore National Laboratory, Livermore, CA 94551, USA

ARTICLE INFO

Article history:
Received 28 May 2021
Received in revised form 8 July 2021
Accepted 19 August 2021
Available online 25 August 2021
Editor: D.F. Geesaman

Keywords:
Superheavy element
Nuclear fission dynamics
Microscopic model calculations

ABSTRACT

Measurements of mass and angular distributions have been made for fission-like outcomes in reactions forming isotopes of flerovium (Z=114), using ^{48}Ca, ^{50}Ti, and ^{54}Cr projectiles. The dominant fast quasifission process, which masks the presence of fusion-fission, has minimum yield at the most backward angles, where the sensitivity to fusion-fission is thus highest. In fitting the backward angle mass spectra, only weak evidence for a component of super-asymmetric fission was found, but a near-symmetric fission component was consistently required for the ^{48}Ca + ^{244}Pu reaction, giving upper limit to the fusion probabilities P_{CN} of $\sim 10^{-2}$, ∼5 times lower than previous results. P_{CN} for the ^{50}Ti reaction was lower than ^{48}Ca, whilst no evidence of fusion-fission was found for the ^{54}Cr reaction.

1. Introduction

An island of superheavy nuclei (SHN) with enhanced stability was predicted in the 1960s, centred at proton and neutron magic numbers Z=114, N=184 [1–3]. All superheavy elements up to Z=118 (oganesson) have now been synthesised [4–9], completing the 7th row of the periodic table of the elements. Measurements of their nuclear decay characteristics test models of nuclear structure [10], whilst atom-by-atom studies of their chemical properties probe the limits of the periodic table [11–16].

SHN are formed by fusion of two lighter nuclei. Capture occurs through kinetic energy dissipation and the "sticking" of their surfaces at contact. However, the probability P_{CN} of moving from this *elongated* contact configuration to the *compact* superheavy compound nucleus (CN) is extremely small [17–20,22]. This is due to strong competition from fast non-equilibrium deep inelastic and quasifission (QF) processes [21–25], typically occurring in $\leqslant 10^{-20}$ s [21,25–29].

The heaviest elements (Z=114-118) have so far been synthesised using the favourable [22,30–32] doubly-magic (Z=20, N=28) neutron-rich ^{48}Ca projectile. In attempting to synthesise elements heavier than oganesson, the insufficiency of target material of elements heavier than Cf [33] requires use of heavier projectiles. Ti to Ni beams have been used, but so far without success [34–38], sug-

* Corresponding author.
E-mail address: kaushik@vecc.gov.in (K. Banerjee).

[1] Presently at Variable Energy Cyclotron Centre, 1/AF, Bidhan Nagar, Kolkata-700064, India.
[2] Presently at Department of Physics, School of Mathematical and Physical Sciences, Central University of Kerala, Kasaragod 671314, India.
[3] Advanced Technology Institute, University of Surrey, Guildford, Surrey, GU2 7XH, United Kingdom.

https://doi.org/10.1016/j.physletb.2021.136601

gesting that P_{CN} values of these projectiles are significantly smaller than for ^{48}Ca [39–41].

Even if a heavy CN is formed by fusion, it is much more likely to undergo fission [i.e., fusion-fission (FF)] than evaporate neutrons to form the desired SHN. The small probability of surviving fission W_{sur} severely inhibits the synthesis of SHN.

The SHN cross-section σ_{SHN} at centre-of-mass energy E is written [42] as the sum over angular momentum $J\hbar$ of the capture cross-section $\sigma_{cap}(E, J)$ multiplied by $P_{CN}(E, J)$ and $W_{sur}(E^*, J)$:

$$\sigma_{SHN}(E) = \sum_J \sigma_{cap}(E, J) P_{CN}(E, J) W_{sur}(E^*, J). \qquad (1)$$

Here E^* is the CN excitation energy above the ground state. At a given E, averaging over the relatively low J in near-barrier capture reactions, this equation simplifies to

$$\sigma_{SHN}(E) = \sigma_{cap}(E).P_{CN}(E).W_{sur}(E^*). \qquad (2)$$

The dominance of FF over particle evaporation for the heavy CN means that essentially $\sigma_{cap}.P_{CN} \simeq \sigma_{FF}$ and hence Eq. (2) can be simplified to $\sigma_{SHN} \simeq \sigma_{FF}.W_{sur}$. If σ_{cap} and σ_{SHN} are already measured, determination of σ_{FF} would thus quantify *both* P_{CN} and W_{sur}. The difficulty is that fusion-fission observables in general overlap [41] with those of the much more likely quasifission process. Various experimental approaches have attempted to overcome this problem [17–20,22,43–46].

These methods generally require knowledge of the mass distribution of the fusion-fission yield. Early empirical conclusions [47], later supported by calculations [48,49], led to the expectation that mass distributions (although being mass-asymmetric) would be within ±20-25 mass units of mass-symmetry [20]. However, recent calculations [50–57] indicate that a super-asymmetric fission decay (with one fragment near ^{208}Pb) has the lowest fission barrier. This would be swamped by the peak in the quasifission yield found at similar masses [28,41,46,58,59].

An experimental technique with high sensitivity to *both* near-symmetric and super-asymmetric fission could address *three* key issues: (i) determination of the mass distribution for superheavy CN fission, informing models of fission; (ii) determining the suppression of SHN cross sections by quasifission, to optimise the choice of reactions and guide dynamical models; (iii) quantifying the competition between neutron evaporation and fission, giving information on fission barrier heights, ground-state shell effects, and thus the location of the magic numbers in the region of SHN [60].

2. Experimental details

Measurements to investigate fusion-fission for three reactions forming isotopes of flerovium were carried out at the ANU Heavy Ion Accelerator Facility using the CUBE detector system [22,27,61,62]. Flerovium compound nuclei having mass numbers 292, 288, and 286 were formed in the reactions ^{48}Ca + ^{244}Pu, ^{50}Ti + ^{238}U, and ^{54}Cr + ^{232}Th respectively, at beam energies from 0.95 to ∼1.15 of their calculated capture barrier energies V_B (192.6, 212.5, and 231.1 MeV respectively) [63]. Targets comprised 50-160 μg/cm^2 of the actinide isotope (enriched to > 97%), supported on 115-280 μg/cm^2 Al/Ti backing foils [64]. Coincident binary reaction products were detected in two of three position-sensitive multi-wire proportional counters [27,62]. Angular coverage was 10° ≤ θ ≤ 80° on one side of the beam axis, and 53° ≤ θ ≤ 169° on the other. Large yields from fission of target-like nuclei were rejected by selecting fission fragments emitted back-to-back in the centre-of-mass (c.m.) frame using the deduced velocity components [27,61] of the nucleus undergoing fission.

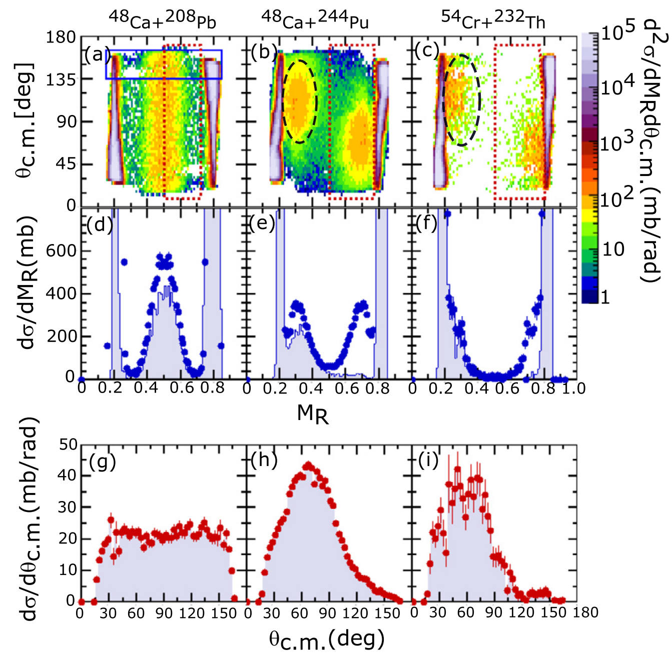

Fig. 1. (a-c) Mass ratio versus angle distributions (MADs) for the binary fragments for ^{48}Ca + ^{208}Pb from Ref. [22] and for ^{48}Ca + ^{244}Pu and ^{54}Cr + ^{232}Th, measured in this work. The fission fragments for ^{48}Ca + ^{208}Pb centred around M_R=0.5 (vertical dashed line) do not vary with angle, characteristic of fusion-fission. The other two reactions are dominated by quasifission with projectile-like (dashed ellipse) and target-like fragments. Total M_R projections are shown by blue points in (d)-(f), and for 135° ≤ $\theta_{c.m.}$ ≤ 165° (scaled up by 4) by shaded histograms. Angular distributions (g) to (i) correspond to the red dashed gates in (a)-(c), showing the strong focusing in angle of fast quasifission in (h) and (i).

3. Data analysis and results

Following energy loss corrections [64] carried out iteratively, the c.m. velocity vectors of the *binary fragments* enable determination of the mass-ratio M_R (the mass of one fragment divided by their sum) and fragment c.m. angles $\theta_{c.m.}$, allowing mass-angle distributions (MADs) to be generated [27,62]. With cross section normalization using sub-barrier elastic scattering [22] the MADs represent the double differential cross section $d^2\sigma/dM_R d\theta_{c.m.}$ as a function of M_R and $\theta_{c.m.}$. Examples are shown in Fig. 1(a)-(c), for beam energies close to the calculated V_B in each reaction.

These MADs show two main groups of events: *scattering* centred around the projectile ($M_R \simeq 0.2$) and target ($M_R \simeq 0.8$) mass-ratios, with angular distributions characteristic of elastic scattering, and binary *fission-like* events following capture, seen at M_R values between those of the projectile and target. It has been demonstrated in Refs. [26,27] that the mass-angle distribution of the binary fission-like events provides information about the time evolution of the nucleus formed following contact. Two quasifission components have been identified: (i) fission soon after contact (fast quasifission), with very little mass exchange and fragment masses close to the target/projectile masses (e.g. dashed ellipses in Fig. 1); (ii) fission much later in the evolution (slow quasifission [59]) but before the formation of a compact CN, with M_R close to 0.5.

For ^{48}Ca + ^{208}Pb at E/V_B = 1.01 [22], the fission-like events in Fig.1(a) are centred at mass-symmetry (M_R = 0.5). The projected total M_R spectrum [blue points in Fig. 1(d)] and the backward angle M_R spectrum 135° ≤ $\theta_{c.m.}$ ≤ 165° (shaded histogram) show the same characteristics. Furthermore, the angular distribution $d\sigma/d\theta_{c.m.}$ for the heavy fragment (0.5 ≤ M_R ≤ 0.72), shown in Fig.1(g), is symmetric about $\theta_{c.m.}$ = 90°. These are all characteristics of fusion-fission, where no “memory” of the projectile, target

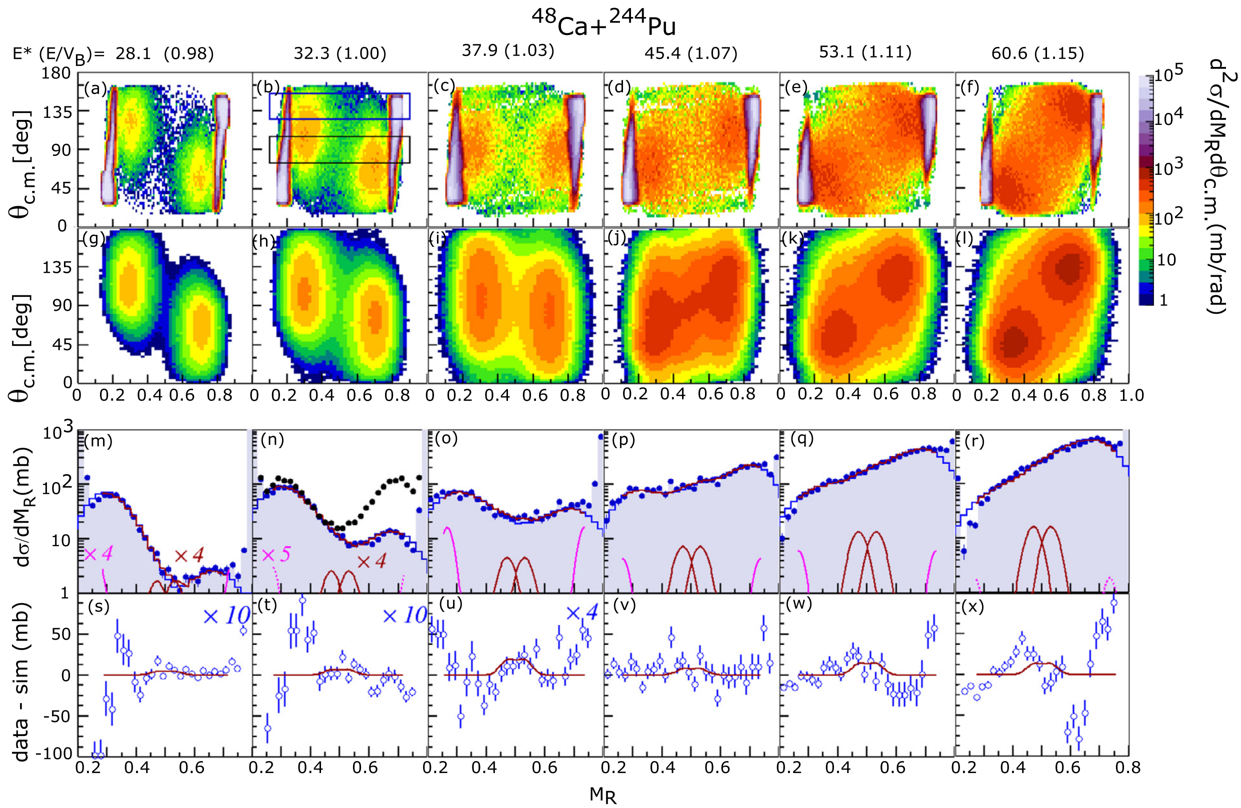

Fig. 2. (a)-(f) Measured MADs for ^{48}Ca + ^{244}Pu at the indicated excitation energy E^* and E/V_B. Panels (g)-(l) show simulated MADs. (m)-(r) show M_R distributions (blue points) within the range 125° $\leq \theta_{c.m.} \leq$155° [blue rectangle in (b)]. Data for 75° $\leq \theta_{c.m.} \leq$105° [black rectangle in (b)] are compared in (n) (black symbols). The M_R spectra are fitted with the QF simulation (blue line) and two Gaussians for super-asymmetric (magenta) and near-symmetric (brown) fusion-fission (only plotted within the fitting range). At most energies, optimum fits needed a near-symmetric fission component (solid brown Gaussians). For the super-asymmetric fusion-fission, upper limits are shown by the dotted Gaussians. The total fits for the near-symmetric fusion-fission are shown by brown histograms. Best-fit Gaussians are scaled by the indicated factors for visibility. (s)-(x) are the difference plots between the experimental M_R data and its simulated counterpart. The near-symmetric fusion-fission components obtained from the fits are shown by brown curves.

mass, and direction remains, and no fission mass-angle correlation appears in the MAD.

MADs for the ^{48}Ca + ^{244}Pu and ^{54}Cr + ^{232}Th reactions at E/V$_B$=1.00 and 0.99 respectively are shown in Fig. 1(b),(c). Results for ^{50}Ti + ^{238}U are qualitatively similar (see Supplemental Material [68]). The characteristics of fission-like events in these reactions are very different from the ^{48}Ca + ^{208}Pb reaction. The peak yield (dashed ellipse) is far from mass-symmetry, also seen in the projected M_R spectra in Fig 1(e) and (f). The angular distributions of the heavy fragments in Fig.1(h) and (i) are sharply peaked in angle. This asymmetry about $\theta_{c.m.}$ = 90° is also demonstrated by the asymmetric M_R distributions for 135° $\leq \theta_{c.m.} \leq$ 165°, shown by the shaded histograms in Fig. 1(e) and (f). All these characteristics are associated with a mass-angle correlation in the MADs, indicating a fast quasifission reaction with a "memory" of the initial collision.

The high statistics for the ^{48}Ca + ^{244}Pu MADs [e.g. Fig. 1(b)] give insights into the origins of the near-symmetric fission events. Unlike ^{48}Ca + ^{208}Pb, where near-symmetric yields populate all angles consistent with long sticking times, the yield for ^{48}Ca + ^{244}Pu is clustered around $\theta_{c.m.}$ = 90° [Fig. 1(b)] as it largely results from the overlap of the broad distributions of fast quasi-fission (projectile-like and target-like) fragments. Yields from fusion-fission must however be present as SHN have been observed [66,67] in reactions of ^{48}Ca with ^{244}Pu. The challenge therefore is to extract the fusion-fission events amidst the dominant fast QF yields. This has been addressed using a new method presented in the following sections.

3.1. Determining the angular region of maximum sensitivity

The overall MAD characteristics and their change with E/V$_B$ for ^{48}Ca + ^{244}Pu, ^{50}Ti + ^{238}U and ^{54}Cr + ^{232}Th are very similar. MADs for ^{48}Ca + ^{244}Pu are shown in Fig.2(a)-(f); the others are shown in the Supplemental material [68]. At the lowest E/V$_B$, the yield of light quasifission fragments (M_R < 0.5) is lowest at forward angles, and of heavy fragments (M_R > 0.5) at backward angles. As E/V$_B$ and the mean angular momentum increases, the light quasifission fragments move to more forward angles as expected [64]. The fast quasifission yield is always minimal at either extreme forward or extreme backward angles, depending on the fragment mass and beam energy. For maximum sensitivity, in particular away from mass-symmetry, a search for fusion-fission should thus be made far from $\theta_{c.m.}$ = 90°.

The backward angle (125° $\leq \theta_{c.m.} \leq$ 155°) M_R distributions are shown in Fig. 2(m)-(r). Fission events are cleanly separated from quasielastic and deep inelastic events for 0.25 $\leq M_R \leq$ 0.75. The peak in the fast quasifission yield moves from M_R= 0.3 to 0.7 with increasing energy. Since in fusion-fission the yields of the light and heavy fragments at any angle must be identical, at least one of the two fusion-fission fragments will be in a region of low quasifission yield. This is not the case around 90° [black points in Fig.2(n)], demonstrating the advantage in selecting angles far from 90° to find the fusion-fission component. The rest of this Letter will therefore concentrate on the backward angle M_R spectra (blue points) to determine the fusion-fission component.

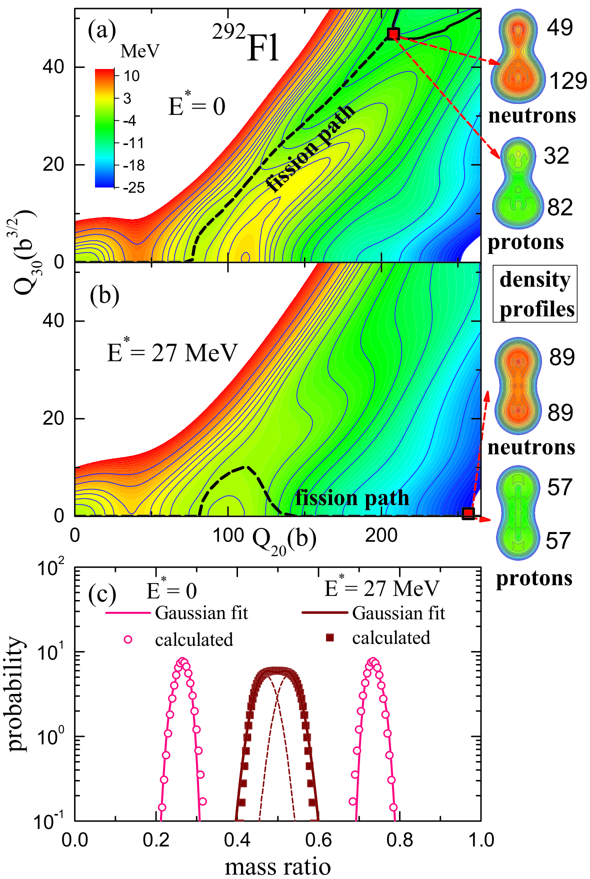

Fig. 3. Free energy surface for ^{292}Fl in elongation (Q_{20}) and mass-asymmetry (Q_{30}) coordinates at (a) zero and (b) 27 MeV excitation. Dashed blue lines show the most likely fission paths. Typical fragment density distributions at the most probable fragmentation are shown to the right. Corresponding calculated fission M_R distributions with Gaussians fits are shown in panel (c) (see text).

3.2. Microscopic calculations

Determining the extremely small contribution of fusion-fission to mass distributions that are dominated by quasi-fission would be made easier if guided by theory. Microscopic calculations of Helmholtz free energy surfaces (FES) is the most suitable tool available for predicting fusion-fission characteristics at non-zero excitation energies. Calculations for ^{292}Fl at two different E^* were therefore carried out to predict whether near-symmetric or super-asymmetric fusion-fission is expected at the measured excitation energies. The nuclear energy density functional formalism at finite-temperature [69,70] is employed to calculate FES in the two-dimensional collective space of multipole moments Q_{20} and Q_{30} representing elongation and mass-asymmetry, respectively. The SkM* parametrization [71] of the Skyrme functional was used to obtain the mean field nucleon-nucleon interaction. Nuclear pairing interactions were included within the Hartree-Fock-Bogoliubov approach [72], and the corresponding strengths were determined from the density-dependent mixed pairing interaction [73]. The FES at E^* = 0 and at 27 MeV are shown in Fig. 3(a) and (b) respectively. At $E^* = 0$ the fission path (dashed line) is highly mass-asymmetric, with the heavy fragment near ^{208}Pb, as found previously [51,52]. In contrast, at E^*=27 MeV, the FES shows little evidence of the super-asymmetric pathway, but rather dominance of fission near mass-symmetry. However, multi-chance fission could result in the presence of both decays in experimental spectra.

Mass-ratio distributions of ^{292}Fl were calculated [74] for both fission decays, as shown by symbols in Fig. 3(c). These distributions could be quite well represented by pairs of Gaussians, as indicated by the curves. The means $\overline{MR}_{peak1}$, $\overline{MR}_{peak2}$, and common standard deviation σ_{MR} of the fitted Gaussians obtained from the present work (for ^{48}Ca+ ^{244}Pu) and from mass distributions reported in Refs. [48,49] (for all systems) for near-symmetric fission are shown in Table 1. Since microscopic calculation takes considerable computation time, an approximation was made for super-asymmetric fission, where Gaussians parameters were determined from the calculated mass distribution of ^{48}Ca + ^{244}Pu for all the three reactions (see Table 1).

Evidence for such near-symmetric or super-asymmetric fission is not clearly visible in the backward angle mass-ratio spectra [Fig.2(m)-(r)]. Since the fusion-fission component is evidently small, a fitting procedure must be applied to extract this component. For the fit, first the smooth quasifission M_R spectrum must be calculated as described below.

3.3. Quasifission simulation and fitting of M_R spectra

The quasifission events were generated using a Monte Carlo simulation of mass and angle evolution [24–27,29,65]. Simultaneous fitting of the M_R and $\theta_{c.m.}$ projections defined the model parameters (see Supplemental Material [68]). The simulated MADs for ^{48}Ca+ ^{244}Pu are shown in Fig.2(g)-(l). Note that the model does not generate narrow mass peaks that are predicted for fusion-fission.

These simulated QF mass distributions provide a consistent description of the measured quasi-fission mass distribution at the wide range of measured angles and beam energies as seen in Fig. 2. They were used to fit the backward angle M_R spectra in Fig. 2(m)-(r) together with a fusion-fission component. The fits were performed by optimising the weighting of the QF distribution (blue histogram) and either the near-symmetric (brown) or super-asymmetric (magenta) fusion-fission components approximated by pairs of Gaussians as specified in Table 1. Fits for the ^{48}Ca reaction are discussed here in detail, whilst fits for ^{50}Ti and ^{54}Cr induced reactions can be found in the Supplemental Material [68].

3.4. Fitting for near-symmetric fusion-fission

Fits of the backward angle M_R spectra for the near-symmetric fission and separately the Gaussian components are shown by brown curves in Fig. 2(m)-(r) for ^{48}Ca + ^{244}Pu. The difference between the measured M_R distribution in the angular region $125° \leq \theta_{c.m.} \leq 155°$ and the fitted quasifission simulation is shown on a linear scale in Fig. 2(s)-(x). Noticeable deviations from the zero level are observed in the mass symmetric region for the ^{48}Ca + ^{244}Pu reaction. The optimum fits obtained for near-symmetric fission are also plotted.

3.5. Fitting for super-asymmetric fusion-fission

The Gaussian components, from the fits for super-asymmetric fission (magenta lines) are also shown Fig. 2(m)-(r) within the M_R fitting range. Optimum values obtained for the Gaussian components are shown by the solid lines, whereas upper limits are represented by the dotted lines.

Large variations from the zero levels can be observed in Fig. 2(s)-(x) in the super-asymmetric mass region $M_R \sim 0.28$ and 0.72. However the magnitudes near $M_R \sim 0.28$ generally do not match those near $M_R \sim 0.72$. These are thus likely from imperfections in the quasifission simulation and not due to the presence of a super-asymmetric fusion-fission component.

Table 1
Parameters for the near-symmetric and super-asymmetric fusion-fission M_R distribution. $\overline{MR}_{peak1}$, $\overline{MR}_{peak2}$ are the means of two peaks and σ_{MR} is the common standard deviation.

Reaction	Near-symmetric				Super-asymmetric			
	$\overline{MR}_{peak1}$	$\overline{MR}_{peak2}$	σ_{MR}	Ref.	$\overline{MR}_{peak1}$	$\overline{MR}_{peak2}$	σ_{MR}	Ref.
^{48}Ca + ^{244}Pu	0.470	0.527	0.026	This work	0.266	0.734	0.018	This work
^{48}Ca + ^{244}Pu	0.463	0.537	0.017	[48,49]	–	–	–	–
^{50}Ti + ^{238}U	0.469	0.531	0.018	[48,49]	0.269	0.745	0.018	Estimation (see text)
^{54}Cr + ^{232}Th	0.472	0.528	0.019	[48,49]	0.271	0.750	0.018	Estimation (see text)

3.6. Determination of fusion-fission cross sections σ_{FF} and the upper limits

A finite yield of near-symmetric fission was returned from the fits of backward angle M_R distributions at all energies for ^{48}Ca + ^{244}Pu. For the other reactions [68], more often upper limits (dotted Gaussians) were obtained. The fusion-fission cross sections σ_{FF} and the upper limits were deduced from the area under the fitted Gaussians extrapolated to the whole angular range taking a constant $d\sigma_{FF}/d\theta$, consistent with ^{48}Ca + ^{208}Pb measurement shown in Figs. 1(a),(g). The σ_{FF} errors were estimated using the fitting errors of the Gaussian weights. Some of the fits returned zero weight for the fusion-fission component. Upper limits were determined in those cases conservatively [75] by the "over-dispersion" criterion $\chi^2 = \chi^2_{min} + \chi^2_{min}/n$ where χ^2, χ^2_{min}, n are the chi-squared over the *full* fit region, the minimum chi-squared, and number of degrees of freedom. Values of χ^2_{min}/n were typically 3.

3.7. Determination of compound nucleus formation probability P_{CN}

P_{CN} values for each reaction, energy, and fission mass distribution were determined using the expression $P_{CN} \cong \sigma_{FF}/\sigma_{cap}$. Values of σ_{cap} were determined from $d\sigma/d\theta_{c.m.}$ of all fission events with $0.5 \lesssim M_R \leq 0.75$ [see Fig.1(h)], extrapolated to 0° and 180° using the quasifission simulation. These σ_{cap} do not include very mass-asymmetric quasifission or deep-inelastic events which lie outside the selected M_R range [22]. Their interpretation will be published elsewhere [76].

P_{CN} values for near-symmetric and super-asymmetric fusion-fission are presented by filled points in Fig. 4(a) and (b) respectively. Since the fusion-fission component is a small fraction of the total, the experimental fit uncertainties (error bars) can be very large. For those fits returning σ_{FF} = 0 (P_{CN} = 0), for visibility the data points have been plotted on the x-axis, at P_{CN}=10^{-4}. P_{CN} values with error bars inconsistent with zero are highlighted with a "halo" around the data point.

For near-symmetric fission [Fig. 4(a)], the fits for ^{48}Ca + ^{244}Pu returned P_{CN} (filled circles) values of typically 10^{-2}, with error bars inconsistent with zero. The sensitivity of the extracted P_{CN} values to the width of the Gaussians used in the fitting process was evaluated by using those calculated in Ref. [48] (see Table 1). The P_{CN} values shift by less than the symbol size [68].

The (upper limit) P_{CN} values from previous work [17], extracted from measured fragment mass-total kinetic energy (TKE) distributions in the angular region around 90°, are shown by the open red circles. The current values (brown filled circles), though consistent with the previous values taken as upper limits [17], are lower typically by a factor of 5. The extracted P_{CN} values would be even lower if the experimental σ_{cap} also included very mass-asymmetric quasifission events outside the selected M_R range of 0.5 - 0.75. If local shell structures enhanced the quasifission [77–81] yield in the same mass region as the fusion-fission, this would also reduce the extracted fusion-fission yield. For these reasons the P_{CN} values determined in this work should be considered upper limits. Using the back angle mass distributions has allowed this limit to be reduced by a factor of 5 compared to previous work [17].

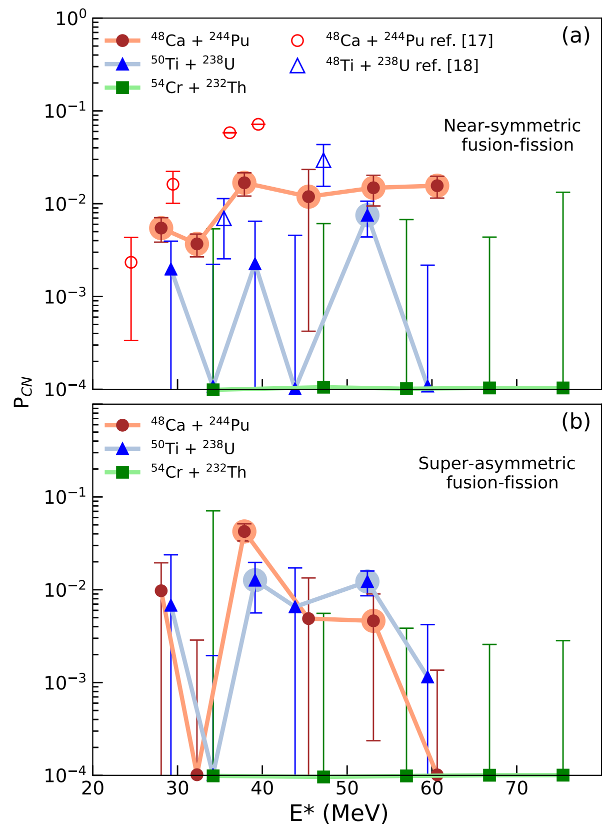

Fig. 4. Compound nucleus formation probability P_{CN} vs. E* for the ^{48}Ca + ^{244}Pu, ^{50}Ti + ^{238}U and ^{54}Cr + ^{232}Th reactions for (a) near-symmetric and (b) super-asymmetric fission. For visibility, fitted values of P_{CN}= 0 are plotted on the x-axis at 10^{-4}. P_{CN} values with error bars inconsistent with zero are highlighted by "halos". Previous P_{CN} values from Refs. [17,18] are also shown.

For ^{50}Ti + ^{238}U, the P_{CN} values for the near-symmetric mode [blue filled triangles in Fig. 4(a)] show more scatter, and are lower than for ^{48}Ca at all E^*. They are also significantly lower on average than the previously determined upper limits [18] for ^{48}Ti + ^{238}U, shown by open triangles in Fig. 4(a). For ^{54}Cr + ^{232}Th, all the extracted P_{CN} values are consistent with zero. These findings are consistent with the expectations that P_{CN} values decrease with increasing target-projectile charge products.

For the super-asymmetric results shown in Fig. 4(b), only four P_{CN} values are inconsistent with zero, and show larger fluctuations compared with the P_{CN} values for the symmetric mode [Fig. 4(a)]. This is likely to be because the simulations of the fast quasifission yield (Fig. 2 third row) fail to match experiment in the most sensitive region of low quasifission yield. Inclusion of additional physical effects in the simulation (such as sequential fission) should improve the model. Experimentally, the low yield of either heavy or light fast quasifission fragments at backward angles results in much better sensitivity to super-asymmetric fission than for measurements closer to $\theta_{c.m.}$ = 90°. This offers opportunities to search for super asymmetric fission though the combination of higher statistics data and improved quasi-fission simulations particularly in the mass-asymmetric region.

4. Conclusion

In summary, extensive measurements of mass and angular distributions from 20° to 160° have been made for fission-like outcomes in the ^{48}Ca + ^{244}Pu, ^{50}Ti + ^{238}U, and ^{54}Cr + ^{232}Th reactions forming isotopes of flerovium (Z=114). The dominant fast quasifission process, which masks the presence of fusion-fission, has minimum yield at angles far from 90° to the beam axis. Measurements at these angles therefore give the highest sensitivity to fusion-fission, and forms the basis of the new method of determining fusion-fission yields presented here. Fitting the backward angle mass distributions with a simulated quasifission and fusion-fission component allowed access to the fusion-fission cross sections. Evidence for the presence of super asymmetric fusion-fission is very weak. On the other hand, the fits consistently required a contribution of near-symmetric fusion-fission of $\sim$ 1% for the ^{48}Ca + ^{244}Pu reaction. Though still considered an upper limit, the fusion probability P_{CN} of $< 10^{-2}$ is $\sim$5 times lower than previous (upper limit) P_{CN} values [17]. For the ^{50}Ti + ^{238}U reaction, P_{CN} is significantly lower, whilst no evidence of fusion-fission is seen for the ^{54}Cr + ^{232}Th reaction. This work demonstrates that high levels of sensitivity to fusion-fission can be achieved from high-statistics measurements of mass distributions at backward angles, close to the beam axis. This opens up a new experimental approach to determine P_{CN}, and the SHN fission mass distribution, advancing understanding of the reaction mechanisms in heavy elements synthesis.

Declaration of competing interest

The authors declare that they have no known competing financial interests or personal relationships that could have appeared to influence the work reported in this paper.

Acknowledgement

The authors acknowledge the Australian Research Council for support through Discovery grants DP170102318, DP190100256, DP200100601. Financial support for accelerator operations was provided by NCRIS through the HIA project. The authors acknowledge the support of the German Academic Exchange Service (DAAD) via funds of the German Federal Ministry of Education and Research (BMBF). The authors would like to thank Prof. Nicolae Carjan of JINR Dubna for providing calculated mass distribution data of Fl nuclei. The authors are grateful to Prof. W. Loveland for providing the ^{238}U target. Computing support came from the Lawrence Livermore National Laboratory (LLNL) Institutional Computing Grand Challenge program.

Appendix A. Supplementary material

Supplementary material related to this article can be found online at https://doi.org/10.1016/j.physletb.2021.136601.

References

[1] William D. Myers, Wladyslaw J. Swiatecki, Nucl. Phys. 81 (1966) 1.
[2] A. Sobiczewski, F.A. Gareev, B.N. Kalinkin, Phys. Lett. 22 (1996) 500.
[3] V.M. Strutinsky, Nucl. Phys. A 95 (1967) 420.
[4] S. Hofmann, S.N. Dmitriev, C. Fahlander, J.M. Gates, J.B. Roberto, H. Sakai, Pure Appl. Chem. 90 (11) (2018) 1773–1832.
[5] Yuri Oganessian, J. Phys. G, Nucl. Part. Phys. 34 (2007) R165.
[6] Yu.Ts. Oganessian, V.K. Utyonkov, Yu.V. Lobanov, F.Sh. Abdullin, A.N. Polyakov, R.N. Sagaidak, I.V. Shirokovsky, Yu.S. Tsyganov, A.A. Voinov, G.G. Gulbekian, S.L. Bogomolov, B.N. Gikal, A.N. Mezentsev, S. Iliev, V.G. Subbotin, A.M. Sukhov, K. Subotic, V.I. Zagrebaev, G.K. Vostokin, M.G. Itkis, K.J. Moody, J.B. Patin, D.A. Shaughnessy, M.A. Stoyer, N.J. Stoyer, P.A. Wilk, J.M. Kenneally, J.H. Landrum, J.F. Wild, R.W. Lougheed, Phys. Rev. C 74 (2006) 044602.
[7] Yu.Ts. Oganessian, F.Sh. Abdullin, P.D. Bailey, D.E. Benker, M.E. Bennett, S.N. Dmitriev, J.G. Ezold, J.H. Hamilton, R.A. Henderson, M.G. Itkis, Yu.V. Lobanov, A.N. Mezentsev, K.J. Moody, S.L. Nelson, A.N. Polyakov, C.E. Porter, A.V. Ramayya, F.D. Riley, J.B. Roberto, M.A. Ryabinin, K.P. Rykaczewski, R.N. Sagaidak, D.A. Shaughnessy, I.V. Shirokovsky, M.A. Stoyer, V.G. Subbotin, R. Sudowe, A.M. Sukhov, Yu.S. Tsyganov, V.K. Utyonkov, A.A. Voinov, G.K. Vostokin, P.A. Wilk, Phys. Rev. Lett. 104 (2010) 142502.
[8] Yu.Ts. Oganessian, F.Sh. Abdullin, C. Alexander, J. Binder, R.A. Boll, S.N. Dmitriev, J. Ezold, K. Felker, J.M. Gostic, R.K. Grzywacz, J.H. Hamilton, R.A. Henderson, M.G. Itkis, K. Miernik, D. Miller, K.J. Moody, A.N. Polyakov, A.V. Ramayya, J.B. Roberto, M.A. Ryabinin, K.P. Rykaczewski, R.N. Sagaidak, D.A. Shaughnessy, I.V. Shirokovsky, M.V. Shumeiko, M.A. Stoyer, N.J. Stoyer, V.G. Subbotin, A.M. Sukhov, Yu.S. Tsyganov, V.K. Utyonkov, A.A. Voinov, G.K. Vostokin, Phys. Rev. Lett. 109 (2012) 162501.
[9] K. Morita, K. Morimoto, D. Kaji, T. Akiyama, S. Goto, H. Haba, E. Ideguchi, R. Kanungo, K. Katori, H. Koura, H. Kudo, T. Ohnishi, A. Ozawa, T. Suda, K. Sueki, H. Xu, T. Yamaguchi, A. Yoneda, A. Yoshida, Y. Zhao, J. Phys. Soc. Jpn. 73 (2004) 2593.
[10] S.A. Giuliani, Z. Matheson, W. Nazarewicz, E. Olsen, P.-G. Reinhard, J. Sadhukhan, B. Schuetrumpf, N. Schunck, P. Schwerdtfeger, Rev. Mod. Phys. 91 (2019) 011001.
[11] P. Schwerdtfeger, O.R. Smits, P. Pyykkö, Nat. Rev. Chem. 4 (2020) 359.
[12] W. Nazarewicz, Nat. Phys. 14 (2018) 537.
[13] V. Pershina, Radiochim. Acta 107 (2019) 833.
[14] A. Türler, V. Pershina, Chem. Rev. 113 (2013) 1237.
[15] A. Türler, R. Eichler, A. Yakushev, Nucl. Phys. A 944 (2015) 640.
[16] Y. Nagame, J.V. Kratz, M. del Schä, Nucl. Phys. A 944 (2015) 614.
[17] E.M. Kozulin, G.N. Knyazheva, I.M. Itkis, M.G. Itkis, A.A. Bogachev, E.V. Chernysheva, L. Krupa, F. Hanappe, O. Dorvaux, L. Stuttgé, W.H. Trzaska, C. Schmitt, G. Chubarian, Phys. Rev. C 90 (2014) 054608.
[18] E.M. Kozulin, G.N. Knyazheva, K.V. Novikov, I.M. Itkis, M.G. Itkis, S.N. Dmitriev, Yu.Ts. Oganessian, A.A. Bogachev, N.I. Kozulina, I. Harca, W.H. Trzaska, T.K. Ghosh, Phys. Rev. C 94 (2016) 054613.
[19] E.M. Kozulin, G.N. Knyazheva, T.K. Ghosh, A. Sen, I.M. Itkis, M.G. Itkis, K.V. Novikov, I.N. Diatlov, I.V. Pchelintsev, C. Bhattacharya, S. Bhattacharya, K. Banerjee, E.O. Saveleva, I.V. Vorobiev, Phys. Rev. C 99 (2019) 014616.
[20] I.M. Itkis, E.M. Kozulin, M.G. Itkis, G.N. Knyazheva, A.A. Bogachev, E.V. Chernysheva, L. Krupa, Yu.Ts. Oganessian, V.I. Zagrebaev, A.Ya. Rusanov, F. Goennenwein, O. Dorvaux, L. Stuttgé, F. Hanappe, E. Vardaci, E. de Goés Brennand, Phys. Rev. C 83 (2011) 064613.
[21] D.J. Hinde, M. Dasgupta, E.C. Simpson, Prog. Part. Nucl. Phys. 118 (2021) 103856.
[22] K. Banerjee, D.J. Hinde, M. Dasgupta, E.C. Simpson, D.Y. Jeung, C. Simenel, B.M.A. Swinton-Bland, E. Williams, I.P. Carter, K.J. Cook, H.M. David, Ch.E. Düllmann, J. Khuyagbaatar, B. Kindler, B. Lommel, E. Prasad, C. Sengupta, J.F. Smith, K. Vo-Phuoc, J. Walshe, A. Yakushev, Phys. Rev. Lett. 122 (2019) 232503.
[23] B.B. Back, R.R. Betts, J.E. Gindler, B.D. Wilkins, S. Saini, M.B. Tsang, C.K. Gelbke, W.G. Lynch, M.A. McMahan, P.A. Baisden, Phys. Rev. C 32 (1985) 195.
[24] J. Toke, B. Bock, G.X. Dai, A. Gobbi, S. Gralla, K.D. Hildenbrand, J. Kuzminski, W.F.J. Müller, A. Olmi, H. Stelzer, Nucl. Phys. A 440 (1985) 327.
[25] W.Q. Shen, J. Albinski, A. Gobbi, S. Gralla, K.D. Hildenbrand, N.J. Kuzminski, W.F.J. Müller, H. Stelzer, J. Toke, B.B. Back, S. Bjørnholm, S.P. Sørensen, Phys. Rev. C 36 (1987) 115.
[26] R. du Rietz, D.J. Hinde, M. Dasgupta, R.G. Thomas, L.R. Gasques, M. Evers, N. Lobanov, A. Wakhle, Phys. Rev. Lett. 106 (2011) 052701.
[27] R. du Rietz, E. Williams, D.J. Hinde, M. Dasgupta, M. Evers, C.J. Lin, D.H. Luong, C. Simenel, A. Wakhle, Phys. Rev. C 88 (2013) 054618.
[28] A. Wakhle, C. Simenel, D.J. Hinde, M. Dasgupta, M. Evers, D.H. Luong, R. du Rietz, E. Williams, Phys. Rev. Lett. 113 (2014) 182502.
[29] E. Prasad, D.J. Hinde, E. Williams, M. Dasgupta, I.P. Carter, K.J. Cook, D.Y. Jeung, D.H. Luong, C.S. Palshetkar, D.C. Rafferty, K. Ramachandran, C. Simenel, A. Wakhle, Phys. Rev. C 96 (2017) 034608.
[30] P. Armbruster, Y.K. Agarwal, W. Bruchle, M. Brugger, J.P. Dufour, H. Gäggeler, F.P. Hessberger, S. Hofmann, P. Lemmertz, G. Münzenberg, K. Poppensieker, W. Reisdorf, M. Schädel, K.-H. Schmidt, J.H.R. Schneider, W.F.W. Schneider, K. Sümmerer, D. Vermeulen, G. Wirth, A. Ghiorso, K.E. Gregorich, D. Lee, M. Leino, K.J. Moody, G.T. Seaborg, R.B. Welch, P. Wilmarth, S. Yashita, C. Frink, N. Greulich, G. Herrmann, U. Hickmann, N. Hildebrand, J.V. Kratz, N. Trautmann, M.M. Fowler, D.C. Hoffman, W.R. Daniels, H.R. von Gunten, H. Dornhofer, Phys. Rev. Lett. 54 (1985) 406.

[31] Yu.Ts. Oganessian, H. Bruchertseifer, G.V. Buklanov, V.I. Chepigin, Choi Val Sek, B. Eichler, K.A. Gavrilov, H. Gaeggeler, Yu.S. Korotkin, O.A. Orlova, T. Reetz, W. Seidel, G.M. Ter-akopian, S.P. Tretyakova, I. Zvara, Nucl. Phys. A 294 (1978) 213.
[32] C. Simenel, D.J. Hinde, R. du Rietz, M. Dasgupta, M. Evers, C.J. Lin, D.H. Luong, A. Wakhle, Phys. Lett. B 710 (2012) 607.
[33] J. Roberto, C. Alexander, R. Boll, J. Burns, J. Ezold, L. Felker, S. Hogle, K. Rykaczewski, Nucl. Phys. A 944 (2015) 99.
[34] Yu.Ts. Oganessian, V.K. Utyonkov, Yu.V. Lobanov, F.Sh. Abdullin, A.N. Polyakov, R.N. Sagaidak, I.V. Shirokovsky, Yu.S. Tsyganov, A.A. Voinov, A.N. Mezentsev, V.G. Subbotin, A.M. Sukhov, K. Subotic, V.I. Zagrebaev, S.N. Dmitriev, R.A. Henderson, K.J. Moody, J.M. Kenneally, J.H. Landrum, D.A. Shaughnessy, M.A. Stoyer, N.J. Stoyer, P.A. Wilk, Phys. Rev. C 79 (2009) 024603.
[35] S. Hofmann, D. Ackermann, S. Antalic, V.F. Comas, S. Heinz, J.A. Heredia, F.P. Heßberger, J. Khuyagbaatar, B. Kindler, I. Kojouharov, M. Leino, B. Lommel, R. Mann, K. Nishio, A.G. Popeko, S. Saro, J. Uusitalo, M. Venhart, A.V. Yeremin, GSI Sci. Rep. 2008 (2009) 131.
[36] S. Hofmann, S. Heinz, D. Ackermann, S. Antalic, W. Barth, H.G. Burkhard, V.F. Comas, L. Dahl, K. Eberhardt, J. Gostic, R. Grzywacz, R.A. Henderson, J.A. Heredia, F.P. Heßberger, J.M. Kenneally, B. Kindler, I. Kojouharov, R. Lang, M. Leino, B. Lommel, R. Mann, J. Maurer, K. Miernik, D. Miller, K.J. Moody, G. Münzenberg, S.L. Nelson, K. Nishio, A.G. Popeko, J.B. Roberto, J. Runke, K.P. Rykaczewski, S. Saro, D.A. Shaughnessy, M.A. Stoyer, P. Thörle-Pospiech, K. Tinschert, N. Trautmann, J. Uusitalo, P.A. Wilk, A.V. Yeremin, GSI Sci. Rep. 2011 (2012) 205.
[37] J. Khuyagbaatar, A. Yakushev, Ch.E. Düllmann, H. Nitsche, J. Roberto, D. Ackermann, L.-L. Andersson, M. Asai, H. Brand, M. Block, D.M. Cox, M. Dasgupta, X. Derkx, A. Di Nitto, J. Dvorak, K. Eberhardt, P.A. Ellison, N.E. Esker, J. Even, M. Evers, C. Fahlander, U. Forsberg, J.M. Gates, N. Gharibyan, K.E. Gregorich, P. Golubev, O. Gothe, J.H. Hamilton, D.J. Hinde, W. Hartmann, R.-D. Herzberg, F.P. Heßberger, J. Hoffmann, R. Hollinger, A. Hübner, E. Jäger, J. Jeppsson, B. Kindler, S. Klein, I. Kojouharov, J.V. Kratz, J. Krier, N. Kurz, S. Lahiri, B. Lommel, M. Maiti, K. Miernik, S. Minami, A. Mistry, C. Mokry, J.P. Omtvedt, G.K. Pang, P. Papadakis, I. Pysmenetska, D. Renisch, D. Rudolph, J. Runke, K. Rykaczewski, L.G. Sarmiento, M. Schädel, B. Schausten, D.A. Shaughnessy, A. Semchenkov, J. Steiner, P. Steinegger, P. Thörle-Pospiech, E.E. Tereshatov, T. Torres De Heidenreich, N. Trautmann, A. Türler, J. Uusitalo, D. Ward, N. Wiehl, M. Wegrzecki, V. Yakusheva, GSI Sci. Rep. 2012 (2013) 131.
[38] J. Khuyagbaatar, A. Yakushev, Ch.E. Düllmann, D. Ackermann, L.-L. Andersson, M. Asai, M. Block, R.A. Boll, H. Brand, D.M. Cox, M. Dasgupta, X. Derkx, A. Di Nitto, K. Eberhardt, J. Even, M. Evers, C. Fahlander, U. Forsberg, J.M. Gates, N. Gharibyan, P. Golubev, K.E. Gregorich, J.H. Hamilton, W. Hartmann, R.-D. Herzberg, F.P. Heßberger, D.J. Hinde, J. Hoffmann, R. Hollinger, A. Hübner, E. Jäger, B. Kindler, J.V. Kratz, J. Krier, N. Kurz, M. Laatiaoui, S. Lahiri, R. Lang, B. Lommel, M. Maiti, K. Miernik, S. Minami, A.K. Mistry, C. Mokry, H. Nitsche, J.P. Omtvedt, G.K. Pang, P. Papadakis, D. Renisch, J. Roberto, D. Rudolph, J. Runke, K.P. Rykaczewski, L.G. Sarmiento, M. Schädel, B. Schausten, A. Semchenkov, D.A. Shaughnessy, P. Steinegger, J. Steiner, E.E. Tereshatov, P. Thörle-Pospiech, K. Tinschert, T. Torres De Heidenreich, N. Trautmann, A. Türler, J. Uusitalo, M. Wegrzecki, N. Wiehl, S.M. Van Cleve, V. Yakusheva, Phys. Rev. C 102 (2020) 064602.
[39] J. Khuyagbaatar, EPJ Web Conf. 163 (2017) 00030.
[40] V. Zagrebaev, W. Greiner, Phys. Rev. C 78 (2008) 034610.
[41] M.G. Itkis, E. Vardaci, I.M. Itkis, G.N. Khyazheva, E.M. Kozulin, Nucl. Phys. A 944 (2015) 204.
[42] G.G. Adamian, N.V. Antonenko, W. Scheid, V.V. Volkov, Nuovo Cimento A 110 (1997) 1143.
[43] R.S. Naik, W. Loveland, P.H. Sprunger, A.M. Vinodkumar, D. Peterson, C.L. Jiang, S. Zhu, X. Tang, E.F. Moore, P. Chowdhury, Phys. Rev. C 76 (2007) 054604.
[44] W. Loveland, J. Phys. Conf. Ser. 420 (2013) 012004.
[45] R. Yanez, W. Loveland, J.S. Barrett, L. Yao, B.B. Back, S. Zhu, T.L. Khoo, Phys. Rev. C 88 (2013) 014606.
[46] M. Morjean, D.J. Hinde, C. Simenel, D.Y. Jeung, M. Airiau, K.J. Cook, M. Dasgupta, A. Drouart, D. Jacquet, S. Kalkal, C.S. Palshetkar, E. Prasad, D. Rafferty, E.C. Simpson, L. Tassan-Got, K. Vo-Phuoc, E. Williams, Phys. Rev. Lett. 119 (2017) 222502.
[47] M.G. Itkis, Yu.Ts. Oganessian, E.M. Kozulin, A.A. Bogatchev, I.M. Itkis, M. Jandel, J. Klimen, G.N. Kniajeva, N.A. Kondratiev, I.V. Korzyukov, L. Krupa, I.V. Pokrovski, V.A. Ponmarenko, E.V. Prokorova, A.Ya. Rusanov, V.M. Voskresenski, F. Haneppe, B. Benoit, T. Materna, N. Rowley, L. Stuttge, G. Giardina, K.J. Moody, in: Proceedings of the International Workshop on Fusion Dynamics at the Extremes, Dubna, Russia, vol. 93, 2000.
[48] N. Carjan, F.A. Ivanyuk, Yu.Ts. Oganessian, Nucl. Phys. A 968 (2017) 453.
[49] N. Carjan, F.A. Ivanyuk, Yu.Ts. Oganessian, Phys. Rev. C 99 (2019) 064606.
[50] D.N. Poenaru, R.A. Gherghescu, W. Greiner, Phys. Rev. Lett. 107 (2011) 062503.
[51] M. Warda, A.Z. deb, L.M. Robledo, Phys. Rev. C 98 (2018) 041602(R).
[52] Z. Matheson, S. Giuliani, W. Nazarewicz, J. Sadhukhan, N. Schunck, Phys. Rev. C 99 (2019) 041304(R).
[53] G. Scamps, C. Simenel, Phys. Rev. C 100 (2019) 041602R.
[54] D.N. Poenaru, R.A. Gherghescu, Phys. Rev. C 97 (2018) 044621.
[55] Y.L. Zhang, Y.Z. Wang, Phys. Rev. C 97 (2018) 014318.
[56] K.P. Santhosh, C. Nithya, Phys. Rev. C 97 (2018) 064616.
[57] C. Ishizuka, X. Zhang, M.D. Usang, F.A. Ivanyuk, S. Chiba, Phys. Rev. C 101 (2020) 011601R.
[58] K. Nishio, S. Mitsuoka, I. Nishinaka, H. Makii, Y. Wakabayashi, H. Ikezoe, K. Hirose, T. Ohtsuki, Y. Aritomo, S. Hofmann, Phys. Rev. C 86 (2012) 034608.
[59] D.J. Hinde, D.Y. Jeung, E. Prasad, A. Wakhle, M. Dasgupta, M. Evers, D.H. Luong, R. du Rietz, C. Simenel, E.C. Simpson, E. Williams, Phys. Rev. C 97 (2018) 024616.
[60] M.G. Itkis, Yu.Ts. Oganessian, V.I. Zagrebaev, Phys. Rev. C 65 (2002) 044602.
[61] D.J. Hinde, M. Dasgupta, J.R. Leigh, J.C. Mein, C.R. Morton, J.O. Newton, H. Timmers, Phys. Rev. C 53 (1996) 1290.
[62] R.G. Thomas, D.J. Hinde, D. Duniec, F. Zenke, M. Das gupta, M.L. Brown, M. Evers, L.R. Gasques, M.D. Rodriguez, A. Diaz-Torres, Phys. Rev. C 77 (2008) 034610.
[63] W.J. Światecki, K. Siwek-Wilczyńska, J. Wilczynski, Phys. Rev. C 71 (2005) 014602.
[64] H.M. Albers, J. Khuyagbaatar, D.J. Hinde, I.P. Carter, K.J. Cook, M. Dasgupta, Ch.E. Düllmann, K. Eberhardt, D.Y. Jeung, S. Kalkal, B. Kindler, N.R. Lobanov, B. Lommel, C. Mokry, E. Prasad, D.C. Rafferty, J. Runke, K. Sekizawa, C. Sengupta, C. Simenel, E.C. Simpson, J.F. Smith, P. Thörle-Pospiech, N. Trautmann, K. Vo-Phuoc, J. Walshe, E. Williams, A. Yakushev, Phys. Lett. B 808 (2020) 135626.
[65] E. Prasad, A. Wakhle, D.J. Hinde, E. Williams, M. Dasgupta, M. Evers, D.H. Luong, G. Mohanto, C. Simenel, K. Vo-Phuoc, Phys. Rev. C 93 (2016) 024607.
[66] Yu.Ts. Oganessian, V.K. Utyonkov, Yu.V. Lobanov, F.Sh. Abdullin, A.N. Polyakov, I.V. Shirokovsky, Yu.S. Tsyganov, G.G. Gulbekian, S.L. Bogomolov, B.N. Gikal, A.N. Mezentsev, S. Iliev, V.G. Subbotin, A.M. Sukhov, G.V. Buklanov, K. Subotic, M.G. Itkis, K.J. Moody, J.F. Wild, N.J. Stoyer, M.A. Stoyer, R.W. Lougheed, Phys. Rev. Lett. 83 (1999) 3154.
[67] Ch.E. Düllmann, M. Schädel, A. Yakushev, A. Türler, K. Eberhardt, J.V. Kratz, D. Ackermann, L.-L. Andersson, M. Block, W. Brüchle, J. Dvorak, H.G. Essel, P.A. Ellison, J. Even, J.M. Gates, A. Gorshkov, R. Graeger, K.E. Gregorich, W. Hartmann, R.-D. Herzberg, F.P. Heßberger, D. Hild, A. Hübner, E. Jäger, J. Khuyagbaatar, B. Kindler, J. Krier, N. Kurz, S. Lahiri, D. Liebe, B. Lommel, M. Maiti, H. Nitsche, J.P. Omtvedt, E. Parr, D. Rudolph, J. Runke, B. Schausten, E. Schimpf, A. Semchenkov, J. Steiner, P. Thörle-Pospiech, J. Uusitalo, M. Wegrzecki, N. Wieh, Phys. Rev. Lett. 104 (2010) 252701.
[68] See Supplemental Material for an extended discussion of the fitting procedure
[69] J.C. Pei, W. Nazarewicz, J.A. Sheikh, A.K. Kerman, Phys. Rev. Lett. 102 (2009) 192501.
[70] N. Schunck, D. Duke, H. Carr, Phys. Rev. C 91 (2015) 034327.
[71] J. Bartel, P. Quentin, M. Brack, C. Guet, H.-B. Håkansson, Nucl. Phys. A 386 (1982) 79.
[72] P. Ring, P. Schuck, The Nuclear Many-Body Problem, Springer-Verlag, 2000.
[73] J. Dobaczewski, W. Nazarewicz, M.V. Stoitsov, Eur. Phys. J. A 15 (2002) 21.
[74] Jhilam Sadhukhan, Samuel A. Giuliani, Zachary Matheson, Witold Nazarewicz, Phys. Rev. C 101 (2020) 065803.
[75] K.H. Schmidt, C.C. Sahm, K. Pielenz, H.G. Clerc, Z. Phys. A 316 (1984) 19.
[76] K. Banerjee, D.J. Hinde, M. Dasgupta, et al., to be published.
[77] M.G. Itkis, J. Äystö, S. Beghini, A.A. Bogachev, L. Corradi, O. Dorvaux, A. Gadea, G. Giardina, F. Hanappe, I.M. Itkis, M. Jandel, J. Kliman, S.V. Khlebnikov, G.N. Kniajeva, N.A. Kondratiev, E.M. Kozulin, L. Krupa, A. Latina, T. Materna, G. Montagnoli, Yu.Ts. Oganessian, I.V. Pokrovsky, E.V. Prokhorova, N. Rowley, V.A. Rubchenya, A.Ya. Rusanov, R.N. Sagaidak, F. Scarlassara, A.M. Stefanini, L. Stuttge, S. Szilner, M. Trotta, W.H. Trzaska, D.N. Vakhtin, A.M. Vinodkumar, V.M. Voskressenski, V.I. Zagrebaev, Nucl. Phys. A 374 (2004) 136.
[78] K. Nishio, H. Ikezoe, S. Mitsuoka, I. Nishinaka, Y. Nagame, Y. Watanabe, T. Ohtsuki, K. Hirose, S. Hofmann, Phys. Rev. C 77 (2008) 064607.
[79] E.M. Kozulin, G.N. Knyazheva, S.N. Dmitriev, I.M. Itkis, M.G. Itkis, T.A. Loktev, K.V. Novikov, A.N. Baranov, W.H. Trzaska, E. Vardaci, S. Heinz, O. Beliuskina, S.V. Khlebnikov, Phys. Rev. C 89 (2014) 014614.
[80] K. Godbey, A.S. Umar, C. Simenel, Phys. Rev. C 100 (2019) 024610.
[81] A.S. Umar, V.E. Oberacker, C. Simenel, Phys. Rev. C 94 (2016) 024605.